Published in final edited form as:
Dent Mater. 2011 May ; 27(5): 465–477. doi:10.1016/j.dental.2011.01.008.

The use of sodium trimetaphosphate as a biomimetic analog of matrix phosphoproteins for remineralization of artificial caries-like dentin

Yan Liu[1], **Nan Li**[2], **Yipin Qi**[3], **Li-na Niu**[4], **Sally Elshafiy**[5], **Jing Mao**[1], **Lorenzo Breschi**[6], **David H. Pashley**[6], and **Franklin R. Tay**[6,*]

[1]Department of Stomatology, Tongji Hospital, Tongji Medical College, Huazhong University of Science and Technology, Wuhan, China

[2]Department of Osteopedics & Traumatology, Fujian University of Traditional Chinese Medicine, Fujian, China

[3]Department of Operative Dentistry and Endodontics, Guanghua School of Stomatology, Sun Yat-sen University, Guangzhou, China

[4]Department of Prosthodontics, School of Stomatology, Fourth Military Medical University, Xian, China

[5]Departments of Oral Biology and Endodontics, School of Dentistry, Medical College of Georgia, Augusta, Georgia, USA

[6]Department of SAU & FAL, University of Bologna, Bologna, Italy

Abstract

Objectives—This study examined the use of sodium trimetaphosphate (STMP) as a biomimetic analog of matrix phosphoproteins for remineralization of artificial carious-affected dentin.

Methods—Artificial carious lesions with lesion depths of 300±30 μm were created by pH-cycling. 2.5% hydrolyzed STMP was applied to the artificial carious lesions to phosphorylate the partially-demineralized collagen matrix. Half of the STMP-treated specimens were bonded with One-Step. The adhesive and non-adhesive infiltrated specimens were remineralized in a Portland cement-simulated body fluid system containing polyacrylic acid (PAA) to stabilize amorphous calcium phosphate as nanoprecursors. Micro-computed tomography (micro-CT) and transmission electron microscopy (TEM) were used to evaluate the results of remineralization after a 4-month period.

Results—In absence of PAA and STMP as biomimetic analogs (control groups), there was no remineralization irrespective of whether the lesions were infiltrated with adhesive. For the STMP-treated experimental groups immersed in PAA-containing simulated body fluid, specimens without adhesive infiltration were more heavily remineralized than those infiltrated with adhesive. Statistical analysis of the 4-month micro-CT data revealed significant differences in the lesion

[*]**Corresponding author**: Dr. Franklin R. Tay, Department of Endodontics, School of Dentistry, Medical College of Georgia, Augusta, GA 30912-1129, USA. Tel.: +1 706 721 2033; Fax: +1 706 721 6252; ftay@mcg,.edu.

depth, relative mineral content along the lesion surface and changes in ΔZ between the non-adhesive and adhesive experimental groups ($p<0.05$ for all the three parameters). TEM examination indicated that collagen degradation occurred in both the non-adhesive and adhesive control and experimental groups after 4 months of remineralization.

Significance—Biomimetic remineralization using STMP is a promising method to remineralize artificial carious lesions particularly in areas devoid of seed crystallites. Future studies should consider the incorporation of MMP-inhibitors within the partially-demineralized collagen matrix to prevent collagen degradation during remineralization.

Keywords

artificial carious lesion; biomimetic; collagen; degradation; remineralization; sodium trimetaphosphate

1. INTRODUCTION

Carious dentin can be classified into outer caries-infected dentin and inner caries-affected dentin [1]. Contemporary caries management is based on a conservative and preventive approach. This minimum invasive philosophy avoids unnecessary tooth sacrifice and leaves caries-affected dentin as the clinical bonding substrate [1,2]. The bond strength to caries-affected dentin substrate has been reported to be significantly lower than that to noncarious dentin [3–5], which has been mainly attributed to the obliteration of dentinal tubules by acid-resistant mineral crystals, thicker zone of exposed collagen after the application of the adhesive system and the lower stiffness and increased water content of the caries-affected dentin [6–9]. Unlike caries-infected dentin, collagen fibrils of the caries-affected dentin still show intermolecular cross-links [10] and distinct cross-banding patterns when examined by transmission electron microscopy (TEM) [11], and therefore are physiologically remineralizable [1,12,13].

Dentin is a mineralized collagenous tissue formed by matrix-mediated mechanisms. Inorganic polyphosphates play an important role in guiding the nucleation and growth of apatite within the gap zones of collagen fibrils during biomineralization [14]. Sodium trimetaphosphate (STMP, $Na_3P_3O_9$), which has been frequently employed as a chemical phosphorylating reagent in the food industry [15–17], has the potential for phosphorylating type I collagen [18]. Chemical phosphorylation of collagen has been shown to be a possible strategy for directing biomimetic growth of bone-like apatite in simulated body fluid (SBF) [19]. However, only large spherical apatite clusters were formed around STMP-phosphorylated collagen matrices in that study, as there was no sequestering mechanism, such as the use of polyaspartic acid or polyacrylic acid, for stabilizing metastable amorphous calcium phosphates (ACPs) as liquid-like nanoprecursors so that they can penetrate the intrafibrillar water compartments of collagen fibrils [20]. As the dual functional motifs of matrix protein components involved in the biomineralization of collagen are identified [21], both the “amorphous calcium phosphate stabilization motif” and the “apatite templating motif” of matrix proteins involved in collagen mineralization have to be replicated for the potential of biomimetic collagen mineralization to be maximized [22–24]. Recently, it has been shown that the phosphate groups of STMP anions can adsorb on demineralized collagen matrices and form covalent bonds with the latter under an alkaline pH [25]. By using polyacrylic acid (PAA) as the ACP stabilization analog and immobilized STMP as analogs of matrix phosphoproteins within collagen, the authors were able to remineralize resin-bonded dentin with intrafibrillar deposition of nanoapatite around STMP-phosphorylated collagen. The phosphate groups of STMPs immobilized on the collagen

fibrils are thought to attract calcium ions by electrostatic force and direct apatite nucleation within the gap zones of collagen fibrils [26–28].

Caries-affected dentin can extend hundreds of microns below the excavated surface. Based on our previous success on biomimetic remineralization of 5–8 μm incompletely resin-infiltrated demineralized dentin [25], the objective of the present study was to remineralize 300 μm thick STMP-treated, artificial caries-like dentin in presence of PAA in a biomimetic remineralization medium as an ACP stabilization motif. To quantitatively assess the changes of mineral density before and after mineralization, micro-computed tomography (micro-CT) was used to examine the mineralized caries-affected dentin non-destructively in three dimensions. Although micro-CT is valuable for longitudinal assessment of mineral uptake, it cannot delineate between intrafibrillar and extrafibrillar apatite deposition within the collagen fibrils. Thus, transmission electron microscopy (TEM) was used to examine the dimension and hierarchy of apatite deposition within the mineralized collagen matrix. As remineralization was negatively affected by the presence of the bonding agent [29], the null hypothesis tested was that there is no difference in the extent of mineralization between adhesive infiltrated and non-adhesive infiltrated artificial carious lesions.

2. MATERIALS AND METHODS

2.1. Preparation of artificial carious lesions by pH-cycling

Thirty extracted non-carious human third molars were obtained with patient informed consent under a protocol approved by the Human Assurance Committee of the Medical College of Georgia. A 1-mm thick dentin disk devoid of enamel and pulp exposure was prepared by making two parallel cuts perpendicular to the longitudinal axis of each tooth using a low-speed Isomet saw (Buehler, Lake Bluff, IL, USA) under water cooling. The surface for creating the partially-demineralized dentin was polished with 1200-grit silicon carbide paper under running water to create a smooth surface layer. The other surface of each dentin disk, together with the circumferential enamel rim and 1 mm of the peripheral dentin of the polished surface (to serve as mineral references) was painted with two coats of an acid-resistant varnish. A 300±30 μm thick layer of partially-demineralized dentin was created on the uncoated surface by pH-cycling procedure [30] to mimic caries-affected dentin below the excavated surface [31]. After pH-cycling, each disk was sectioned transversely under running water to create two 3-mm wide slabs containing the partially-demineralized dentin.

2.2 Micro-CT scans

To assess the lesion depth and mineral loss, each slab was scanned non-destructively under water using a SkyScan 1174 compact X-ray micro-CT scanner (Micro Photonics, Allentown, PA, USA). A custom-made mold was created for each specimen using a sectioned pipette tip and polyvinylsiloxane impression material to serve as a positioning jig. The latter was attached perpendicularly to the specimen turntable of the micro-CT scanner to acquire the whole image of each slice. As the X-ray source is polychromatic, a 1-mm thick aluminum filter was placed in front of the detector to remove low-energy radiation. Scanning was performed with a spatial resolution of 6.28 μm at 50 kV and 800 μA. Flat-field correction, geometric correction for random movement during the acquisition phase and ring artifact correction during the reconstruction phase were performed to reduce ring artifacts. A 20% beam hardening correction was employed during the reconstruction phase using the NRecon software (Skyscan 1174).

Following image reconstruction, two-dimension virtual slices in the sagittal plane were acquired using the Data Viewer software (Skyscan 1174). The same acquisition and

reconstruction parameters were used when the same slab was re-scanned during subsequent months. The sagittal virtual serial sections derived from each slab were subjected to maximum intensity projection (MIP) with the CTAnalyzer software (Skyscan1174) to obtain a stacked 2-D image (Fig. 1). As the CTAnalyzer only permits individual line scans across an image, the stacked 2-D image was imported into ImageJ (NIH, Bethesda, MD, USA) to produce an overall mineral profile within a standardized volume of interest (VOI) (Fig. 1). A white vertical line was formed extending from the radiopaque, non-demineralized part of the slab surface to the radiolucent lesion surface. This virtual line served as the superimposition reference for mineral profiles obtained during different time periods and eliminated the manifestation of streak artifacts introduced by incorporating a highly radiopaque reference within the specimen [32]. Mineral profiles were determined at exactly the same area (4×1 mm) within the stacked image during the experiment (Fig. 1). The length scale of the ordinate in the overall mineral profile was expressed in micrometers based on the resolution employed during image acquisition. The gray-scale attenuation values in the abscissa was expressing as the relative mineral volume by normalizing the mineral density of the mineralized dentin to 50 vol% mineral density [33]. The output parameters obtained were mineral content profiles of the lesions, lesion depth (μm, being the depth where the relative mineral content was 95% of the mineralized dentin value) and the integrated mineral loss (ΔZ, vol%.μm) as described previously [34].

2.3 STMP pre-treatment and dentin bonding

Based on the baseline micro-CT data, 32 slabs with 300±30 μm lesion depth were selected for the following experiments. Slabs with lesion depths that fell outside this range were rejected. As protein phosphorylation with STMP is usually performed at pH > 11 to open its closed ring structure [35], STMP (Mw 305.9, Sigma-Aldrich, St Louis, MO, USA) was hydrolyzed at pH 12 for 5 h followed by neutralization to pH 7.4 before use. Based on the adsorption characteristics of STMP on demineralized dentin collagen [25], 16 slabs were treated with 2.5 wt% STMP solution for 5 min and randomly divided into two groups (N=8): 1) without adhesive; 2) with adhesive. The other 16 slabs were not treated with hydrolyzed STMP and were designated as the negative controls for the no-adhesive with adhesive infiltrated experimental groups. For both the adhesive experimental group and its corresponding control group, five coats of an acetone-based unfilled adhesive (One-Step, Bisco Inc., Schaumburg, IL, USA) were liberally applied to the artificial carious lesion, allowed to soak in the dark for 1 min to permit as much adhesive infiltration as possible into the thick layer of partially-demineralized dentin [7] and light-polymerized for 20 sec. As the lesions were already partially demineralized, no additional phosphoric acid etchant was employed prior to the application of the two-step etch-and-rinse adhesive. The adhesive infiltrated slabs were stored at 100% relative humidity for 24 h to enable the bonds to mature. Slabs from the non-adhesive groups were stored in deionized water during that period.

2.4 Remineralization medium

A 1 cm diameter, 2 mm thick resin composite disk consisting of a light-polymerizable hydrophilic resin blend (50 wt%), 45 wt% set white Portland cement powder and 5 wt% silanized silica was used as the sustained releasing sources of calcium and hydroxyl ions [23]. The set white Portland cement was prepared by mixing with water in a 0.35 to 1 water-powder ratio, allowed to set completely for 1 week in 100% relative humidity, ground to a fine powder and sieved to retrieve particles that were smaller than 38 μm in diameter. A simulated body fluid (SBF) was prepared by dissolving 136.8 mM NaCl, 4.2 mM $NaHCO_3$, 3.0 mM KCl, 1.0 mM $K_2HPO_4{\cdot}3H_2O$, 1.5 mM $MgCl_2{\cdot}6H_2O$, 2.5 mM $CaCl_2$ and 0.5 mM Na_2SO_4 in deionized water and adding 3.08 mM sodium azide to prevent bacterial growth. The SBF was buffered to pH 7.4 with 0.1 M Tris Base and 0.1 M HCl and served as the

control remineralization medium. For the biomimetic remineralization medium, 500 μg/mL polyacrylic acid (PAA, Mw 1800; Sigma-Aldrich) was added to the SBF and buffered to pH 7.4 to stabilize the amorphous calcium phosphate produced by the interaction of the set Portland cement with SBF in the form of nanoprecursor droplets [22,36].

2.5 Remineralization of artificial carious lesions

Each slab in the experimental and control groups was placed on top of a composite disk inside a glass scintillation vial with lesion surface contacting the composite. This simulated the placement of a composite over the adhesive infiltrated or unbonded lesion but alleviated the difficulty in removing the Portland cement-containing composite during subsequent ultramicrotomy. The assembly was placed inside a glass scintillation vial, which was filled with 15 mL of biomimetic remineralization medium for the two experimental groups or 15 mL of SBF for the two control groups. The specimens were incubated in each medium for four months at 37°C, with the medium refreshed twice every month. The pH was monitored daily so that the value was above 9.5 to enable the formation of apatite instead of octacalcium phosphate from the initially formed amorphous calcium phosphate phase [37]. Each slab was retrieved at monthly intervals (i.e. 1, 2, 3 and 4 months), rinsed briefly with water to remove loose surface precipitates, inserted into the corresponding micro-CT positioning jig, covered with pH-adjusted deionized water (pH 7.4) and scanned with the micro-CT. After scanning, each slab was removed from the positioning jig and returned to the corresponding immersion medium for continuous mineralization.

2.6 Statistical analyses

The 32 slabs with artificial carious lesions (mean lesion depth 300±30 μm) were assigned to the two experimental groups and the two control groups (N=8) by analyzing the slab assignment with one-way ANOVA at $\alpha = 0.05$ to ensure there were no differences in the baseline lesion depths among the four groups prior to the commencement of the experiment.

As there was no remineralization observed in the two control groups, the lesion depths, integrated mineral losses (ΔZs), and the relative mineral contents along the lesion surface at baseline and after 4 months of remineralization in the non-adhesive and adhesive experimental groups were statistically analyzed. As the normality (Shapiro-Wilk test) and homoscedasticity (Levene test) assumptions of the data derived from each of the three parameters appeared to be violated, each parameter was analyzed separately using the Mann-Whitney rank sum test at $\alpha = 0.05$.

2.7 Transmission electron microscopy (TEM)

After remineralization for four months, four specimens from each of the four experimental and control groups were selected for transmission electron microscopy. The selection criteria were that the overall lesion depths and changes in ΔZ were closest to the mean values obtained for that particular group. The slabs were fixed in Karnovsky's fixative, post-fixed in 1% osmium tetroxide, dehydrated in an ascending ethanol series (50–100%), immersed in propylene oxide as a transitional fluid and embedded in epoxy resin.

Non-demineralized thick sections (210–250 nm thick) of the entire artificial carious lesion including part of the mineralized dentin base were first prepared for overall evaluation of the effect of remineralization. The blocks were then trimmed to 1.5 × 1.5 mm for preparation of non-demineralized thin sections (90–110 nm thick). These sections were prepared by diamond knives mounted on a Leica EM UC6 ultramicrotome (Leica Microsystems GmbH, Wetzlar, Germany), collected on single-slot carbon and formvar-coated nickel grids and examined without further staining. After initial examination of the thin sections, selected specimens of interest were demineralized in-situ by placing the grid upside down over a

drop of 0.05 N HCl for 60 sec. After demineralization, each grid was dipped in-and-out of deionized water to remove precipitates and then stained with 1% phosphotungstic acid followed by 2% uranyl acetate to examine the status of collagen within the artificial carious lesions. In addition, two rejected slabs (lesion depths beyond the range required) were completely demineralized in formic acid/sodium formate within one week after preparation of the artificial carious lesions, embedded in epoxy resin as described previously and prepared for stained thin sections for examination of the status of the collagen within the artificial carious lesion prior to remineralization. Examination was performed using a JEM-1230 TEM (JEOL, Tokyo, Japan) at 110 kV.

3. RESULTS

Mineral profiles in the non-adhesive and adhesive control groups (i.e. no STMP treatment and immersion in SBF only) remained relatively constant over the 4-month period (not shown). Figure 2A represents the overall mineral profile changes in the non-adhesive experimental group (i.e. STMP-treated and immersed in SBF containing 500 μg/mL PAA) over the 4-month period. Each profile represents the mean values derived from the eight lesions in that group. The baseline mineral profile indicated that demineralization was incomplete along the lesion surface (relative mineral content 11.1±1.6 vol%). There was a gradient of demineralization from the surface to the base of the lesions (lesion depth 291.4±7.3 μm). The baseline integrated mineral loss from the lesions (ΔZ) was 5312.2±409.6 μm.vol%. After 4 months of biomimetic remineralization, there was a marked increase in the relative mineral content along the surface of the lesions (41.4±6.1 vol%; 50 vol% being the nominal value adopted to represent that of sound mineralized intertubular dentin). The lesion depth was reduced to 77.2±9.4 μm, representing a 73.5±3.0% reduction. After 4 months, ΔZ was reduced to 489.4±153.3 μm.vol%, representing a 90.9±2.5% reduction.

Figure 2B represents the overall mineral profile obtained from the adhesive experimental group. The baseline relative mineral content along the surface of the lesions was 10.8±1.1 vol% and the baseline lesion depth was 291.9±7.0 μm. The baseline ΔZ was 5685.3±248.8 μm.vol%. After 4 months of biomimetic remineralization in the presence of an adhesive layer, there was only a slight increase in the relative mineral content along the lesion surface (21.0±8.7 vol%). The lesion depth was reduced to 138.6±20.9 μm, representing a 52.6±6.7% reduction. The ΔZ was reduced to 2486.9±613.6 μm.vol%, representing a 56.6±9.5% reduction at the end of the 4-month remineralization period.

Changes in lesion depth, relative mineral content along the lesion surface and ΔZ of the non-adhesive and adhesive experimental groups are shown in the Table. The baseline lesion depths of the non-adhesive and adhesive control groups (not shown in the Table) are 289.7±9.6 μm and 294.2±6.3 μm, respectively. There was no significant difference in the baseline lesion depth among the four groups ($p > 0.05$). As there was basically no change in the remineralization parameters in the two control groups after 4 months, they were excluded from the subsequent statistical analyses performed on the 4-month data and only the non-adhesive experimental group was compared with the adhesive experimental group. After 4 months, the lesion depth in the non-adhesive experimental group was significantly smaller than the adhesive experimental group ($p < 0.05$). The relative mineral content along the lesion surface was significantly higher in the non-adhesive experimental group ($p < 0.05$). Remineralization efficacy [$\Delta Z_{\text{baseline}} - \Delta Z_{\text{4 months}})/\Delta Z_{\text{baseline}}$*100%] in the non-adhesive experimental group was also significantly higher than the adhesive experimental group ($p < 0.05$).

Stained, completely laboratory-demineralized "rejected" specimens indicated the collagen fibrils within the entire lesions were intact at baseline and demonstrated stainable cross banding patterns (not shown). Figure 3A is a stacked 2-D micro-CT image taken from the adhesive control group after 4 months of immersion in SBF, the control medium. This composite image represents the overall lesion profile derived from 450–480 superimposed virtual serial sections. Thick sections of the lesion revealed an approximately 300 μm thick zone of partially-demineralized dentin that exhibited a gradient of increasing mineral density from the lesion surface to the base of the lesion. The surface of the lesion contained mostly remnant extrafibrillar seed crystallites (Fig. 3C; see also baseline of Fig. 2B) and exhibited a similar electron density as the dentin surface of a baseline non-remineralized lesion (not shown). Collagen fibrils along the surface 50 μm of the lesion appeared intact in stained demineralized sections (Fig. 3D). However, there was a zone between 50–150 μm from the lesion surface where collagen degradation could be identified (Fig. 3E). Within this zone, the dentinal tubules were considerably widened and distorted (Fig. 3C). Collagen fibrils beyond 150 μm from the lesion surface, however, appeared intact. Lesions taken from the non-adhesive control group were similar in their mineral distribution and appearance (not shown), with the exception that collagen degradation could be identified from the surface and extending 100–150 μm into the lesion. Collagen fibrils beyond 150 μm from the lesion surface also appeared intact.

Artificial carious lesions from both the non-adhesive and adhesive experimental groups exhibited a variable extent of remineralization after 4 months even within a single specimen. A representative example of a remineralized lesion from the non-adhesive experimental group is illustrated in Figures 4 and 5. In Figure 4A, the lesion appeared to be heavily remineralized along its entire length except for a diffuse region adjacent to the non-demineralized enamel and dentin reference (Fig. 4B). Along the lesion surface, the originally sparsely-mineralized collagen matrix became heavily remineralized by the deposition of extrafibrillar and intrafibrillar apatite crystallites (Figs. 4C and 4D). Nevertheless, intrafibrillar remineralization was incomplete when thin sections were examined at high magnifications (Fig. 4E). Those intrafibrillar crystallites appeared as platelets that were between 10–40 nm along their C-axis. Stained demineralized sections of the lesion revealed intact collagen fibrils throughout the lesion without signs of fibrillar degradation (not shown). Figure 5 was taken from the same specimen within the diffuse, less heavily remineralized region (Fig. 5A). At the TEM thick section level, the surface 100 μm of the lesion appeared less electron-dense (Fig. 5B). Distinctive areas of degradation could be recognized along the partially remineralized dentin surface. In those areas, the intertubular collagen matrix completely disappeared (Fig. 5C). At the TEM thin section level, a characteristic collagen remineralization pattern could be identified from those degraded areas. The pattern appeared as islands of dense mineral deposition dispersed within a matrix with sparse mineral deposition (Fig. 5D). The crystallite arrangement in the less electron-dense, sparsely remineralized matrix was random and non-hierarchical. Those densely and sparsely remineralized sites corresponded respectively to areas containing intact collagen and areas with fibrillar unraveling and degradation when the TEM sections were demineralized and stained for further examination (Fig. 5E).

Lesions from the adhesive experimental group were less heavily remineralized than those from the non-adhesive experimental group. Figures 6 and 7 represent different regions taken from the same 4-month old, partially remineralized, adhesive infiltrated lesion. These regions were taken respectively from locations with different radiopacity as identified from the 2-D micro-CT stacked image (Figs. 6A and 7A). In the more radiopaque region, the partially remineralized adhesive infiltrated lesion exhibited a variable degree of electron density when examined at the TEM thick section level (Fig. 6B). The surface of the lesion appeared more heavily mineralized (Fig. 6C) at the TEM thin section level when compared

to a baseline, non-remineralized lesion (Fig. 3C). Intrafibrillar apatite deposition could be identified readily from collagen fibrils along the dentin surface (Fig. 6D). Examination of stained demineralized thin sections revealed intact collagen fibrils throughout the entire lesion (not shown). Hierarchical intrafibrillar deposition could be identified from the more heavily remineralized middle and basal parts of the lesion (Fig. 6E). Nevertheless, intrafibrillar compartments with incomplete apatite deposition could be observed.

Images from Figure 7 were taken from a different location of the same specimen shown in Fig. 6 in which only a faint radiopacity could be discerned within that part of the lesion (Fig. 7A). Both TEM thick and thin sections revealed a sparsely-remineralized zone from the top 50 μm of the lesion (Figs. 7B and 7C). A zone of collagen degradation could be seen beneath the intact surface zone wherein gross degradation of the dentin substrate was present, with areas that were completely devoid of a collagen matrix (Fig. 7C). The recognizable collagen matrix adjacent to those degraded regions was, surprisingly, moderately remineralized. However, the remineralization characteristics of a partially-degraded collagen matrix could be readily discerned from those areas (Fig. 7D). The latter consisted of islands with heavy mineralization dispersed within a matrix with sparse mineralization. Examination of stained demineralized sections confirmed that many of the collagen fibrils in those sparsely remineralized sites were denatured (Fig. 7E). Collagen fibrils beneath the surface 120–150 μm of the lesion were heavily remineralized and appeared intact (not shown).

4. Discussion

A the micro-CT data indicated that there are significant differences in lesion depth, relative mineral content along the dentin surface and changes in ΔZ between the non-adhesive and adhesive experimental groups, the null hypothesis that there is no difference between adhesive infiltrated and non-adhesive infiltrated artificial carious lesions has to be rejected. In the present study, we employed artificial caries-like dentin lesions in the present study to simulate caries-affected dentin. It must be stressed that the two substrates are considerably different. The dentinal tubules in natural caries-affected dentin are occluded with acid-resistant mineral crystals that reduce its permeability to fluid movements [38]. Our experimental setup also did not include bacteria that may be present in the superficial layers of caries-affected dentin, which may alter the outcome of remineralization [39]. These microstructural and composition differences between natural caries-affected dentin and artificial caries-like dentin may result in differences in remineralization efficacy between the two substrates [40]. Thus, further studies are required to confirm the efficacy of the present biomimetic remineralization protocol in remineralizing natural caries-affected dentin.

The biomimetic remineralization protocol employed in the present study incorporates the dual functional motifs of naturally occurring matrix proteins involved in biomineralization [22–24]. The latter is well-regulated and controlled spatially and temporally by noncollagenous matrix proteins. It is well established that the collagen matrix serves as a scaffold for crystal deposition but does not provides a mechanism for nucleation of hydroxyapatite [21]. Acidic matrix proteins with a high affinity for calcium ions and collagen fibrils are responsible for regulating the nucleation and growth of the mineral phase in mineralized hard tissues [21,41]. Both micro-CT and TEM demonstrated that there was no evidence of remineralization in the negative control groups. Amorphous calcium phosphate (ACP) can be formed by the use of set white Portland cement as the source of sustained calcium and hydroxyl ions and SBF as the source of phosphate ions [23]. As there were no biomimetic analogs employed in the control groups, large ACP globules up to 2 μm in diameter were initially formed, which were then transformed to large apatite crystallites that are 200–250 nm along their c-axis [22]. Therefore, there were only precipitations along

the dentin surface as those large apatite crystallites cannot fit in the gap zones between collagen molecules (*ca*. 40 nm wide).

Conventional remineralization of artificial caries-like dentin often involves the use of calcium and phosphate ion-containing solutions in presence of various concentrations of fluoride [42,43]. Such a remineralization mechanism does not rely on spontaneous nucleation of mineral on the organic matrix but rather on epitaxial growth of residual apatite seed crystallites in the partially demineralized carious dentin [44–47]. Thus, only those parts of a collagen matrix where remnant seed crystallites are present and abundant can be effectively remineralized, such as the basal part of a carious lesion. In this regard, the use of conventional remineralization strategies that do not utilize biomimetic analogs is reasonably successful. Although fluoride enhances mineral uptake, it may result in hypermineralization of the lesion surface [42,48] and prevents effective remineralization of the deeper parts of a carious lesion [43]. In the present study, even though fluoride was not used a component of the remineralization medium, a 41.4 ± 6.1 vol% relative mineral content was achieved along the lesion surface in the non-adhesive experimental group (50 vol% being the nominal mineral volume adopted for intact intertubular dentin). This may be accounted for by the ability of STMP to function as templating molecules to attract PAA-stabilized ACP nanoprecursors and to nucleate apatite within the intrafibrillar compartments of the collagen fibrils that were originally depleted of seed crystallites [24,25]. There are two possible reasons why remineralization with the biomimetic approach was incomplete within this surface region. The first is that water from the intrafibrillar compartments of the collagen fibrils was incompletely replaced by the newly formed apatite [49] (Fig. 4E). Although STMP may be bound to demineralized collagen via a electrostatic mechanism and a chemical phosphorylation mechanism [19,25], part of the electrostatically-bound STMP could have diffused out of the collagen matrix during the 4-month remineralization period. The other reason for incomplete remineralization of the surface region in the non-adhesive experimental group is the degradation of the collagen matrix, which will be elaborated in the subsequent parts of the discussion.

The better remineralization efficacy observed in the non-adhesive experimental group over the adhesive experimental group parallels the results reported by Dickens and Flaim [29] when a calcium phosphate remineralization cement was placed over adhesive infiltrated artificial carious lesions in the absence of biomimetic analogs. The results may be interpreted from two different perspectives. From a positive perspective, although it is impossible for an etch-and-rinse adhesive to completely infiltrate a 300 μm thick layer of partially demineralized dentin [7,50,51], a diffusion gradient invariably exists, with better adhesive infiltration along the surface than the basal part of the lesion [52,53]. Beyond the surface where adhesive infiltration is optimal, the subsurface pattern of incomplete infiltration in caries-affected dentin is non-uniform and islands of better adhesive infiltration were found to be dispersed within islands of incomplete resin infiltration in the presence of a silver tracer [54]. As the interfibrillar spaces of the collagen matrix within the top 50 μm of the lesion were better infiltrated by resin, a relatively lower remineralization efficacy in this region may be reasonably expected. From a negative perspective, the presence of an adhesive layer between the remineralization composite and the surface of the adhesive infiltrated dentin hampers the inward diffusion of calcium ions released by the composite. Interaction between the calcium ions and a polymerized resin matrix containing acidic functional groups may also have compromised the penetration of calcium ions into the adhesive infiltrated dentin. These factors may also have contributed to the lower remineralization efficacy in the adhesive experimental group. This does not mean, however, that the surface of the adhesive infiltrated lesion did not remineralized at all. From Fig. 2B, it is apparent that the relative mineral content along the lesion surface increased from approximately 11 vol% to 21 vol%. Transmission electron microscopy also showed that

there was an increase in the intrafibrillar mineral deposition along the surface of the adhesive infiltrated lesions (Fig. 6D vs Fig. 3C). There was also a significant increase in mineral content over basal part (approximately 150–300 μm) of the adhesive infiltrated lesions (Figs. 2B, 6A and 6E). Taken together, it appears that the water-sorbed adhesive layer permitted diffusion of the calcium ions, albeit at a slower rate. Although biomimetc remineralization occured in an adhesive infiltrated lesion, the slower rate of remineralization using a process that relies on diffusion of remineralization components through the adhesive layer resulted in undesirable consequences such as degradation of an intrafibrillar mineral-depleted collagen matrix before optimal remineralization may be effectively accomplished.

The mean baseline relative mineral content along the baseline lesion surface was very low (*ca*. 10 vol%), which corresponded with the TEM result that intrafibrillar minerals were scanty toward the lesion surface (Fig. 3C). As the exposed or incompletely resin-infiltrated collagen unprotected by intrafibrillar minerals could not resist denaturation challenges by endogenous matrix metalloproteinases (MMPs) (Fig. 3E) [55,56], collagen degradation occurred in both the control and experimental groups (Figs. 3E, 5C, 7C). It is also important to note that irrespective of whether the lesions were infiltrated with adhesive, collagen fibrils from the middle and basal portions of the lesion (*ca.* 150–300 μm) did not exhibit signs of degradation. This may be explained by the presence of sufficient remnant extrafibrillar and intrafibrillar apatite crystallites in the collagen matrix that prevented the fossilized MMPs from being functionally active.

In the past, collagen degradation associated with incomplete remineralization has seldom been reported in the literature [57,58]. While a shorter period of remineralization may have accounted for the absence of collagen degradation, it is prudent to mention that the use of microradiography or micro-CT only provided information on mineral density. Understandably, evidence of collagen degradation could only be identified at the ultrastructural level using transmission electron microcopy or micro-Raman spectroscopy (as alteration in peak ratios of amide I to amide III of the collagen matrix) [59,60]. Such data were unavailable in classical remineralization studies. Although polyvinylphosphonic acid, another potential analog of matrix phosphoproteins employed in biomimetic mineralization strategies [22,23] has been shown to possess anti-MMP potential against MMP-9 [61], we have not been able to detect anti-MMP activities in STMP, the biomimetic analog utilized in the present study. In the future, it is necessary to apply MMP inhibitors to thick, partially-demineralized collagen matrices when lengthy periods of remineralization are anticipated. Similar to our previous study [62], it is interesting to note that even structurally-altered dentin collagen is amendable to remineralization in presence of biomimetic analogs that incorporate the dual functional motifs of biomineralization. Nevertheless, degraded collagen cannot be remineralized to the same extent or hierarchical order that is seen in structurally-intact dentin collagen (Figs. 5D, 7D). This result further demonstrates that biomimetic remineralization strategy has the potential to remineralize caries-infected dentin by non-hierarchical deposition of nanoapatite crystallites within the structurally-disintegrated gelatin matrix.

Within the limits of the present study, it may be concluded that biomimetic remineralization using STMP as an analog of matrix phosphoproteins is a promising method to remineralize artificial carious lesions from the perspectives of mineral uptake and ultrastructure. As remineralization in locations without apatite seed crystallites takes a considerably longer time period than that required for epitaxial growth over existing seed crystallites, future studies should consider the incorporation of MMP-inhibitors within the partially-demineralized collagen matrix or MMP-inhibiting resin components into a dentin adhesive. Moreover, as diffusion of remineralization components through an adhesive layer is likely to be hampered by the presence of an adhesive layer, it is worth considering the incorporation

of these components via the use of nanoparticle technology into the partially demineralized collagen matrix prior to the application of the adhesive. This may render the remineralization components more readily accessible to the intertubular collagen matrix and expedite the rate of remineralization before matrix degradation occurs via endogenous MMP activities. Understanding how thick artificial carious lesions respond to biomimetic remineralization will pave the way for more detailed investigations on the development of clinically-relevant delivery systems to remineralize “real” caries-affected dentin.

REFERENCES

1. Fusayama T. Two layers of carious dentin: Diagnosis and treatment. Oper Dent. 1979; 4:63–70. [PubMed: 296808]
2. Marshall GW, Marshall SJ, Kinney JH, Balooch M. The dentin substrate: structure and properties related to bonding. J Dent. 1997; 25:441–458. [PubMed: 9604576]
3. Nakajima M, Sano H, Urabe I, Tagami J, Pashley DH. Bond strengths of single-bottle dentin adhesives to caries-affected dentin. Oper Dent. 2000; 25:2–10. [PubMed: 11203785]
4. Yoshiyama M, Urayama A, Kimochi T, Matsuo T, Pashley DH. Comparison of conventional vs self etching adhesive bonds to caries-affected dentin. Oper Dent. 2000; 25:163–169. [PubMed: 11203811]
5. Wei S, Sadr A, Shimada Y, Tagami J. Effect of caries-affected dentin hardness on the shear bond strength of current adhesives. J Adhes Dent. 2008; 10:431–440. [PubMed: 19189673]
6. Ito S, Saito T, Tay FR, Carvalho RM, Yoshiyama M, Pashley DH. Water content and apparent stiffness of non-caries versus caries-affected human dentin. J Biomed Mater Res B Appl Biomater. 2005; 72:109–116. [PubMed: 15389491]
7. Haj-Ali R, Walker M, Williams K, Wang Y, Spencer P. Histomorphologic characterization of noncarious and caries-affected dentin/adhesive interfaces. J Prosthodont. 2006; 15:82–88. [PubMed: 16650007]
8. Hsu KW, Marshall SJ, Pinzon LM, Watanabe L, Saiz E, Marshall GW. SEM evaluation of resin-carious dentin interfaces formed by two dentin adhesive systems. Dent Mater. 2008; 24:880–887. [PubMed: 18155289]
9. Perdigão J. Dentin bonding-variables related to the clinical situation and the substrate treatment. Dent Mater. 2010; 26:e24–e37. [PubMed: 20005565]
10. Kuboki Y, Tsuzaki M, Sasaki S, Liu CF, Mechanic GL. Location of the intermolecular cross-links in bovine dentin collagen, solubilization with trypsin and isolation of cross-link peptides containing dihydroxylysinonorleucine and pyridinoline. Biochem Biophys Res Commun. 1981; 102:119–126. [PubMed: 7306142]
11. Ogushi K, Fusayama T. Electron microscopic structure of the two layers of carious dentin. J Dent Res. 1975; 54:1019–1026. [PubMed: 1058852]
12. Kuboki Y, Ohgushi K, Fusayama T. Collagen biochemistry of the two layers of carious dentin. J Dent Res. 1977; 56:1233–1237. [PubMed: 272387]
13. Nakornchai S, Atsawasuwan P, Kitamura E, Surarit R, Yamauchi M. Partial biochemical characterisation of collagen in carious dentin of human primary teeth. Arch Oral Biol. 2004; 49:267–273. [PubMed: 15003545]
14. George A, Veis A. Phosphorylated proteins and control over apatite nucleation, crystal growth and inhibition. Chen Rev. 2008; 108:4670–4693.
15. Lee SH, Yang JI, Hong SM, Hahm DH, Lee SY, Kim IH, et al. Phosphorylation of peptides derived from isolated soybean protein: effects on calcium binding, solubility and influx into Caco-2 cells. Biofactors. 2005; 23:121–128. [PubMed: 16410634]
16. Zhang K, Li Y, Ren Y. Research on the phosphorylation of soy protein isolate with sodium tripolyphosphate. J Food Eng. 2007; 79:1233–1237.
17. Leone G, Torricelli P, Giardino R, Barbucci R. New phosphorylated derivatives of carboxymethylcellulose with osteogenic activity. Polym Adv Technol. 2008; 19:824–830.
18. Gunasekaran S. Purifying type I collagen using two papain treatments and reducing and delipidation agents. United States Patent Office. 2003; 6:548. 077.

19. Li X, Chang J. Preparation of bone-like apatite-collagen nanocomposites by a biomimetic process with phosphorylated collagen. J Biomed Mater Res A. 2008; 85:293–300. [PubMed: 17688292]
20. Olszta MJ, Odom DJ, Douglas EP, Gower LB. A new paradigm for biomineral formation: mineralization via an amorphous liquid-phase precursor. Connect Tissue Res. 2003; 44 Suppl. 1:326–334. [PubMed: 12952217]
21. Gajjeraman S, Narayanan K, Hao J, Qin C, George A. Matrix macromolecules in hard tissues control the nucleation and hierarchical assembly of hydroxyapatite. J Biol Chem. 2007; 282:1193–1204. [PubMed: 17052984]
22. Tay FR, Pashley DH. Guided tissue remineralisation of partially demineralised human dentine. Biomaterials. 2008; 29:1127–1137. [PubMed: 18022228]
23. Kim YK, Gu L-S, Bryan TE, Kim JR, Chen L, Liu Y, et al. Mineralization of reconstituted collagen using polyvinylphosphonic acid/polyacrylic acid templating matrix protein analogues in the presence of calcium, phosphate and hydroxyl ions. Biomaterials. 2010; 31:6618–6627. [PubMed: 20621767]
24. Liu Y, Kim YK, Dai L, Li N, Khan S, Pashley DH, et al. Hierarchical and non-hierarchical mineralization of collagen. Biomaterials. 2011; 32:1291–1300. [PubMed: 21040969]
25. Gu LS, Kim J, Kim YK, Liu Y, Dickens SH, Pashley DH, et al. A chemical phosphorylation-inspired design for Type I collagen biomimetic remineralization. Dent Mater. 2010; 26:1077–1089. [PubMed: 20688381]
26. Zhang RY, Ma PX. Porous poly(L-lactic acid)/apatite composites created by biomimetic process. J Biomed Mater Res. 1999; 45:285–293. [PubMed: 10321700]
27. Kikuchi M, Itoh S, Ichinose S, Shinomiya K, Tanaka J. Self-organization mechanism in a bone-like hydroxyapatite/collagen nanocomposite synthesized in vitro and its biological reaction in vivo. Biomaterials. 2001; 22:1705–1711. [PubMed: 11396873]
28. Hartgerink JD, Beniash E, Stupp SI. Self-assembly and mineralization of peptide-amphiphile nanofibers. Science. 2001; 294:1684–1688. [PubMed: 11721046]
29. Dickens SH, Flaim GM. Effect of a bonding agent on in vitro biochemical activities of remineralizing resin-based calcium phosphate cements. Dent Mater. 2008; 24:1273–1280. [PubMed: 18359510]
30. ten Cate JM, Buijs MJ, Damen JJ. pH-cycling of enamel and dentin lesions in the presence of low concentrations of fluoride. Eur J Oral Sci. 1995; 103:362–367. [PubMed: 8747671]
31. Neves Ade A, Coutinho E, Vivan Cardoso M, Jaecques SV, Van Meerbeek B. Micro-CT based quantitative evaluation of caries excavation. Dent Mater. 2010; 26:579–588. [PubMed: 20347481]
32. Barrett JF, Keat N. Artifacts in CT: recognition and avoidance. RadioGraphics. 2004; 24:1679–1691. [PubMed: 15537976]
33. Märten A, Fratzl P, Paris O, Zaslansky P. On the mineral in collagen of human crown dentine. Biomaterials. 2010; 31:5479–5490. [PubMed: 20399496]
34. Gelhard TBFM, Arends J. Microradiography of *in vivo* remineralized lesions in human enamel. J Biol Buccale. 1984; 12:59–65. [PubMed: 6584426]
35. Shen CY. Alkaline hydrolysis of sodium trimetaphosphate in concentrated solutions and its role in built detergents. Ind Eng Chem Prod Res Dev. 1966; 5:272–276.
36. Liou SC, Chen SY, Liu DM. Manipulation of nanoneedle and nanosphere apatite/poly(acrylic acid) nanocomposites. J Biomed Mater Res B Appl Biomater. 2005; 73:117–122. [PubMed: 15672405]
37. Meyer JL, Eanes ED. A thermodynamic analysis of the secondary transition in the spontaneous precipitation of calcium phosphate. Calcif Tissue Res. 1978; 25:209–216. [PubMed: 30523]
38. Pashley EL, Talman R, Horner JA, Pashley DH. Permeability of normal versus carious dentin. Endo Dent Traumatol. 1991; 7:207–211.
39. Sá LT, González-Cabezas C, Cochran MA, Fontana M, Matis BA, Moore BK. Fluoride releasing materials: their anti-cariogenic properties tested in *in vitro* caries models. Oper Dent. 2004; 29:524–531. [PubMed: 15470874]
40. Yang B, Flaim G, Dickens SH. Remineralization of human natural caries and artificial caries-like lesions with an experimental whisker-reinforced ART-composite. Acta Biomater. 2011

41. Tartaix PH, Doulaverakis M, George A, Fisher LW, Butler WT, Qin C, Salih E, Tan M, Fujimoto Y, Spevak L, Boskey AL. In vitro effects of dentin matrix protein-1 on hydroxyapatite formation provide insights into in vivo functions. J Biol Chem. 2004; 279:18115–18120. [PubMed: 14769788]
42. Kawasaki K, Ruben J, Tsuda H, Huysmans MCDNJM, Takagi O. Relationship between mineral distributions in dentin lesions and subsequent remineralization in vitro. Caries Res. 2000; 34:395–403. [PubMed: 11014906]
43. Preston KP, Smith PW, Higham SM. The influence of varying fluoride concentrations on in vitro remineralisation of artificial dentinal lesions with differing lesion morphologies. Arch Oral Biol. 2008; 53:20–26. [PubMed: 17920030]
44. Marion AA, Becker RO. Evidence for epitaxy in the formation of collagen and apatite. Nature. 1970; 226:652–653. [PubMed: 4315552]
45. Koutsoukos PG, Nancollas GH. Crystal growth of calcium phosphates – epitaxial considerations. J Crystal Growth. 1981; 53:10–19.
46. Doi Y, Eanes ED. Transmission electron microscopic study of calcium phosphate formation in supersaturated solutions seeded with apatite. Calcif Tissue Int. 1984; 36:39–47. [PubMed: 6423234]
47. Liu Y, Sethuraman G, Wu W, Nancollas GH, Grynpas M. The crystallization of fluorapatite in the presence of hydroxyapatite seeds and of hydroxyapatite in the presence of fluorapatite seeds. J Colloid Interface Sci. 1997; 186:102–109. [PubMed: 9056310]
48. Baysan A, Lynch E, Ellwood R, Davies R, Petersson L, Borsboom P. Reversal of primary root caries using dentifrices containing 5,000 and 1100 ppm fluoride. Caries Res. 2001; 35:41–46. [PubMed: 11125195]
49. Kim YK, Mai S, Mazzoni A, Liu Y, Tezvergil-Mutluay A, Takahashi K, et al. Biomimetic remineralization as a progressive dehydration mechanism of collagen matrices - Implications in the aging of resin-dentin bonds. Acta Biomater. 2010; 6:3729–3739. [PubMed: 20304110]
50. Spencer P, Wang Y, Katz JL, Misra A. Physicochemical interactions at the dentin/adhesive interface using FTIR chemical imaging. J Biomed Opt. 2005; 10 031104.
51. Zanchi CH, Lund RG, Perrone LR, Ribeiro GA, del Pino FA, Pinto MB, et al. Microtensile bond strength of two-step etch-and-rinse adhesive systems on sound and artificial caries-affected dentin. Am J Dent. 2010; 23:152–156. [PubMed: 20718212]
52. Wang Y, Spencer P. Quantifying adhesive penetration in adhesive/dentin interface using confocal Raman microspectroscopy. J Biomed Mater Res. 2002; 59:46–55. [PubMed: 11745536]
53. Rolland SL, Walls AW, McCabe JF, German MJ. Use of micro-Raman spectroscopy to investigate hybrid layer quality in demineralized root dentine. J Biomed Mater Res B Appl Biomater. 2010; 95:62–68. [PubMed: 20690175]
54. Silva NR, Carvalho RM, Pegoraro LF, Tay FR, Thompson VP. Evaluation of a self-limiting concept in dentinal caries removal. J Dent Res. 2006; 85:282–286. [PubMed: 16498079]
55. Pashley DH, Tay FR, Yiu C, Hashimoto M, Breschi L, Carvalho RM, et al. Collagen degradation by host-derived enzymes during aging. J Dent Res. 2004; 83:216–221. [PubMed: 14981122]
56. Tezvergil-Mutluay A, Agee KA, Hoshika T, Carrilho M, Breschi L, Tjäderhane L, et al. The requirement of zinc and calcium ions for functional MMP activity in demineralized dentin matrices. Dent Mater. 2010; 26:1059–1067. [PubMed: 20688380]
57. Liu Y, Tjäderhane L, Breschi L, Mazzoni A, Li N, Mao J, et al. Limitations in bonding to dentin and experimental strategies to prevent bond degradation. J Dent Res. 2011
58. Liu Y, Mai S, Li N, Yiu CK, Mao J, Pashley DH, et al. Differences between top-down and bottom-up approaches in mineralizing thick, partially demineralized collagen scaffolds. Acta Biomater. 2010
59. Wang Y, Spencer P. Analysis of acid-treated dentin smear debris and smear layers using confocal Raman microspectroscopy. J Biomed Mater Res. 2002; 60:300–308. [PubMed: 11857437]
60. Karan K, Yao X, Xu C, Wang Y. Chemical profile of the dentin substrate in non-carious cervical lesions. Dent Mater. 2009; 25:1205–1212. [PubMed: 19464050]

61. Tezvergil-Mutluay A, Agee KA, Hoshika T, Tay FR, Pashley DH. The inhibitory effect of polyvinylphosphonic acid on functional matrix metalloproteinase activities in human demineralized dentin. Acta Biomater. 2010; 6:4136–4142. [PubMed: 20580949]

62. Mai S, Kim YK, Kim J, Yiu CK, Ling J, Pashley DH, et al. In vitro remineralization of severely compromised bonded dentin. J Dent Res. 2010; 89:405–410. [PubMed: 20173183]

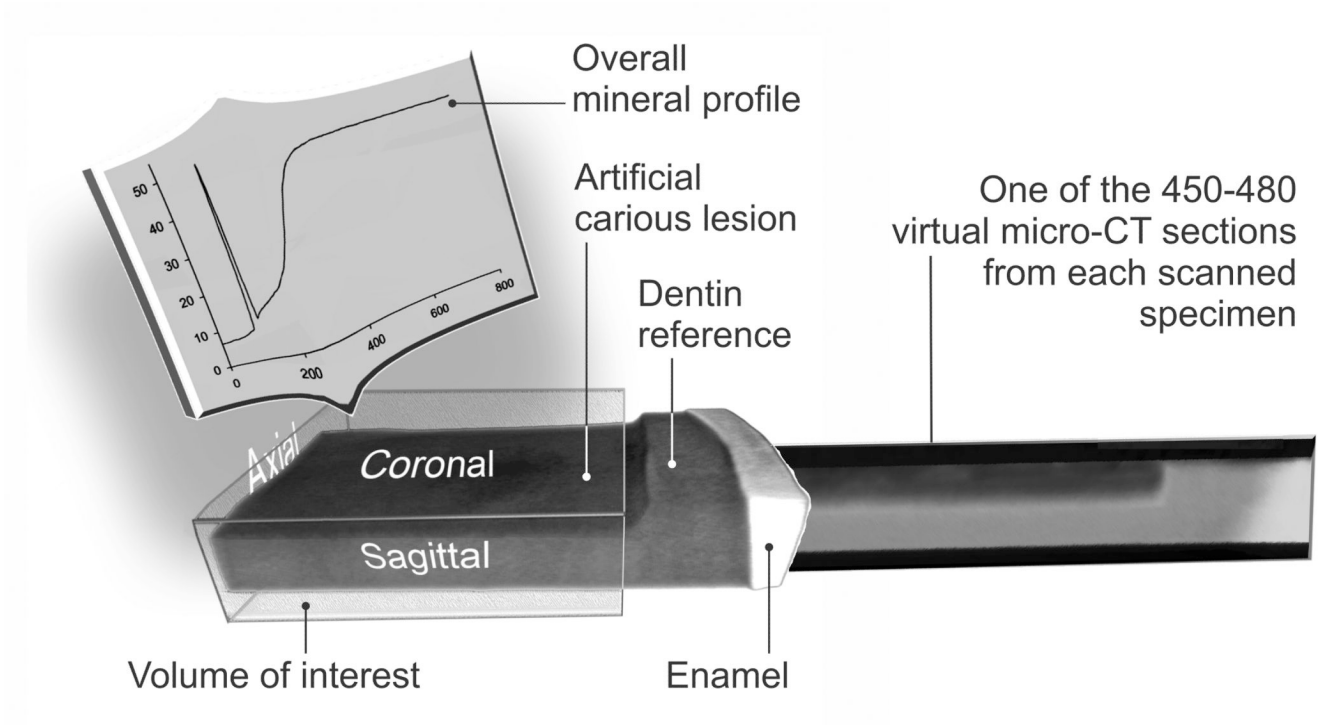

Fig. 1.
A schematic illustrating how the overall mineral profile of an artificial carious lesion was derived from the volume of interest using stacked 2-D micro-CT scanned images.

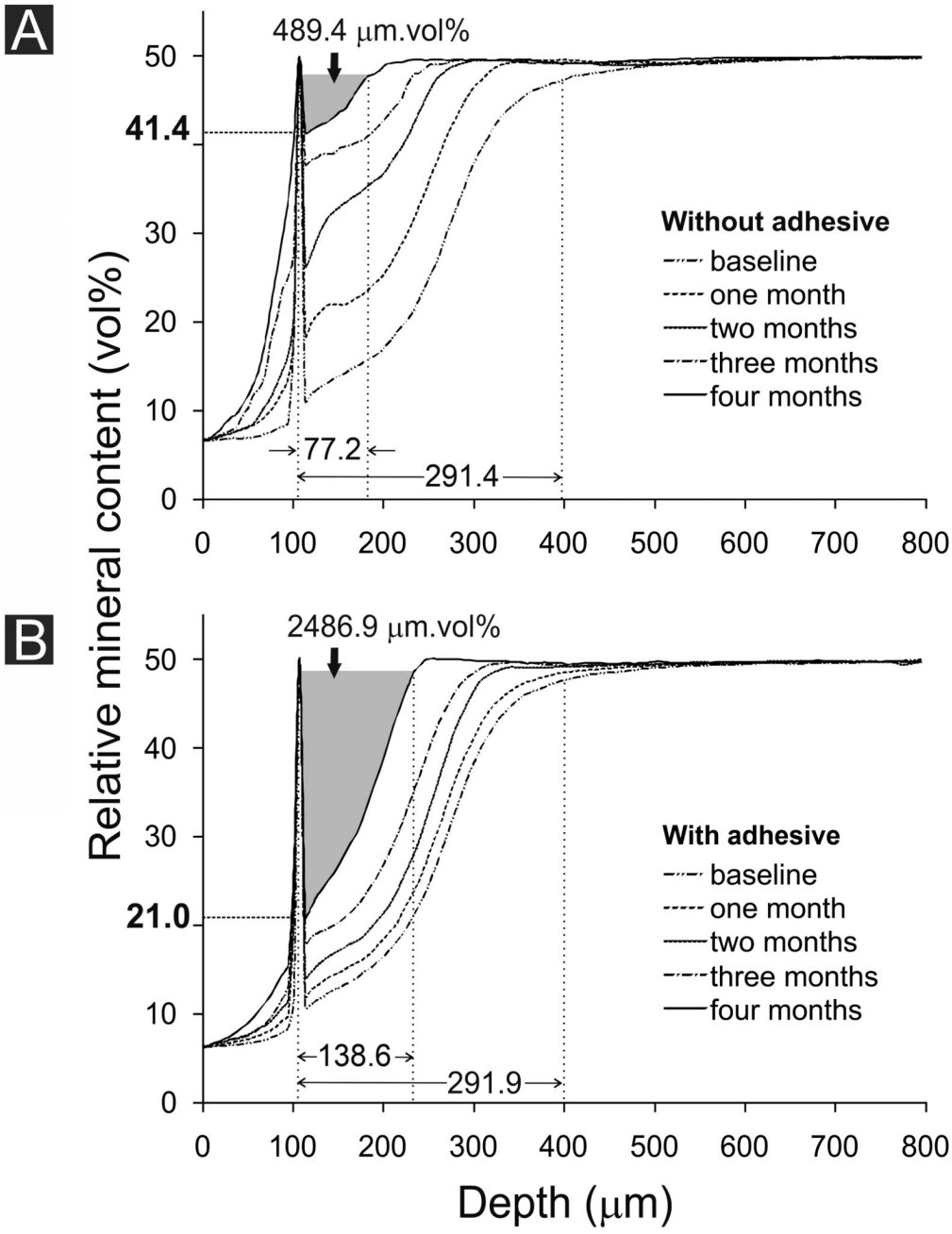

Fig. 2.

Changes in overall mineral profile over time for **A**. Biomimetic remineralization of unbonded artificial carious lesions. **B**. Biomimetic remineralization of artificial caries-like dentin lesions that were infiltrated with One-Step adhesive. The ΔZ for the 4th month in each group is highlighted in gray. The relative mineral content along the lesion surface after the 4th month of remineralization is represented by the bold value along the Y-axis (see Table). Mean baseline lesion depth and mean lesion depth after the 4th month of remineralization are indicated by values above the X-axis (see Table).

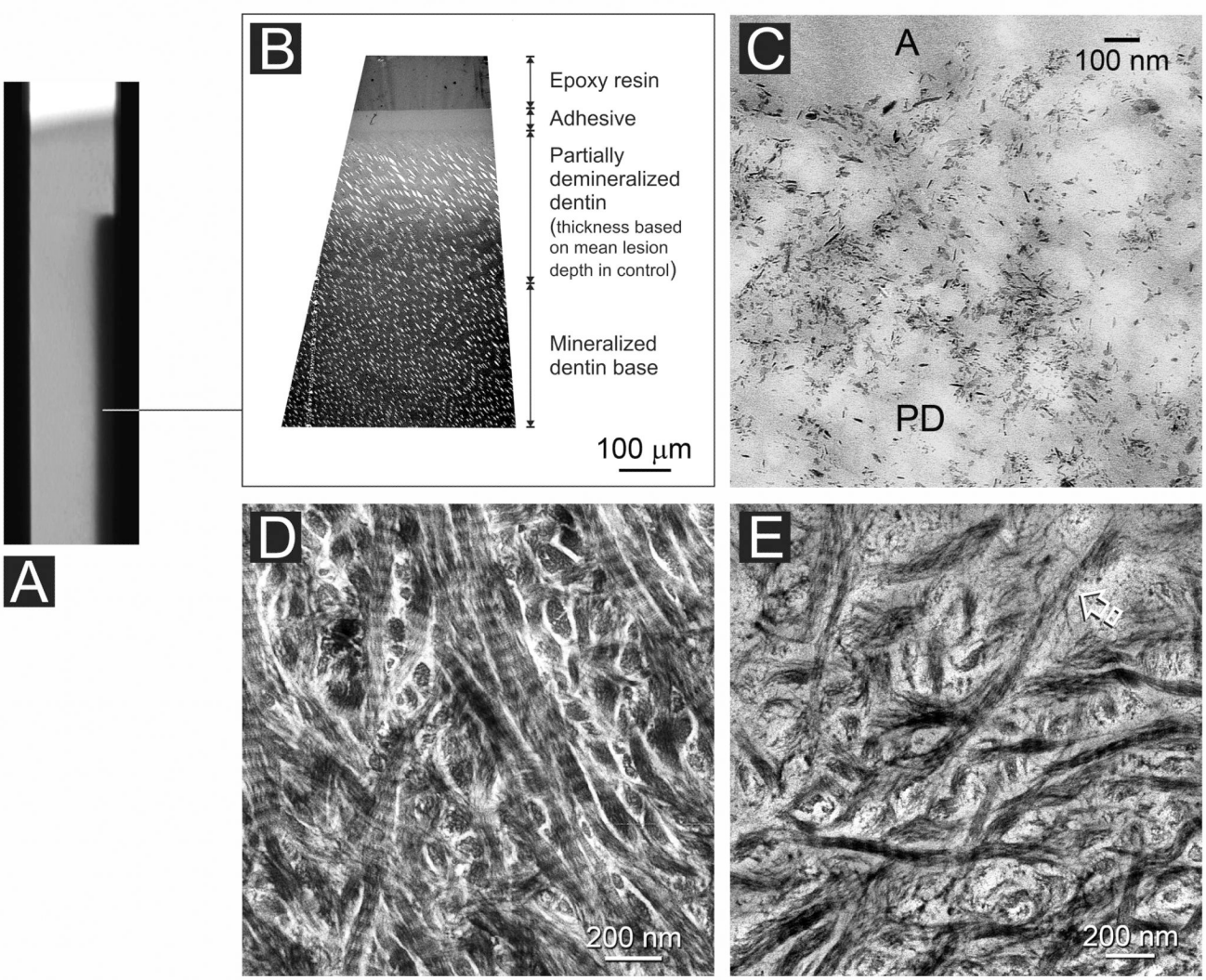

Fig. 3.

Characterization of an adhesive infiltrated artificial caries-like dentin lesion after 4 months of immersion in simulated body fluid (control). **A**. A stacked 2-D micro-CT image representing the lesion profile from 450–480 superimposed virtual serial sections. **B**. Non-demineralized thick section showing absence of remineralization (similar to baseline, not shown). **C**. Non-demineralized thin section showing sparse distribution of remnant seed crystallites along the lesion surface of the partially-demineralized dentin (PD). A: adhesive. **D**. Stained, demineralized thin section showing intact collagen directly beneath the lesion surface where the lesion was better infiltrated by adhesive resin. **E**. Partially-degraded collagen between 50–150 μm from the lesion surface where the distribution of remnant intrafibrillar apatite is not profuse enough to protect the collagen fibrils from degradation.

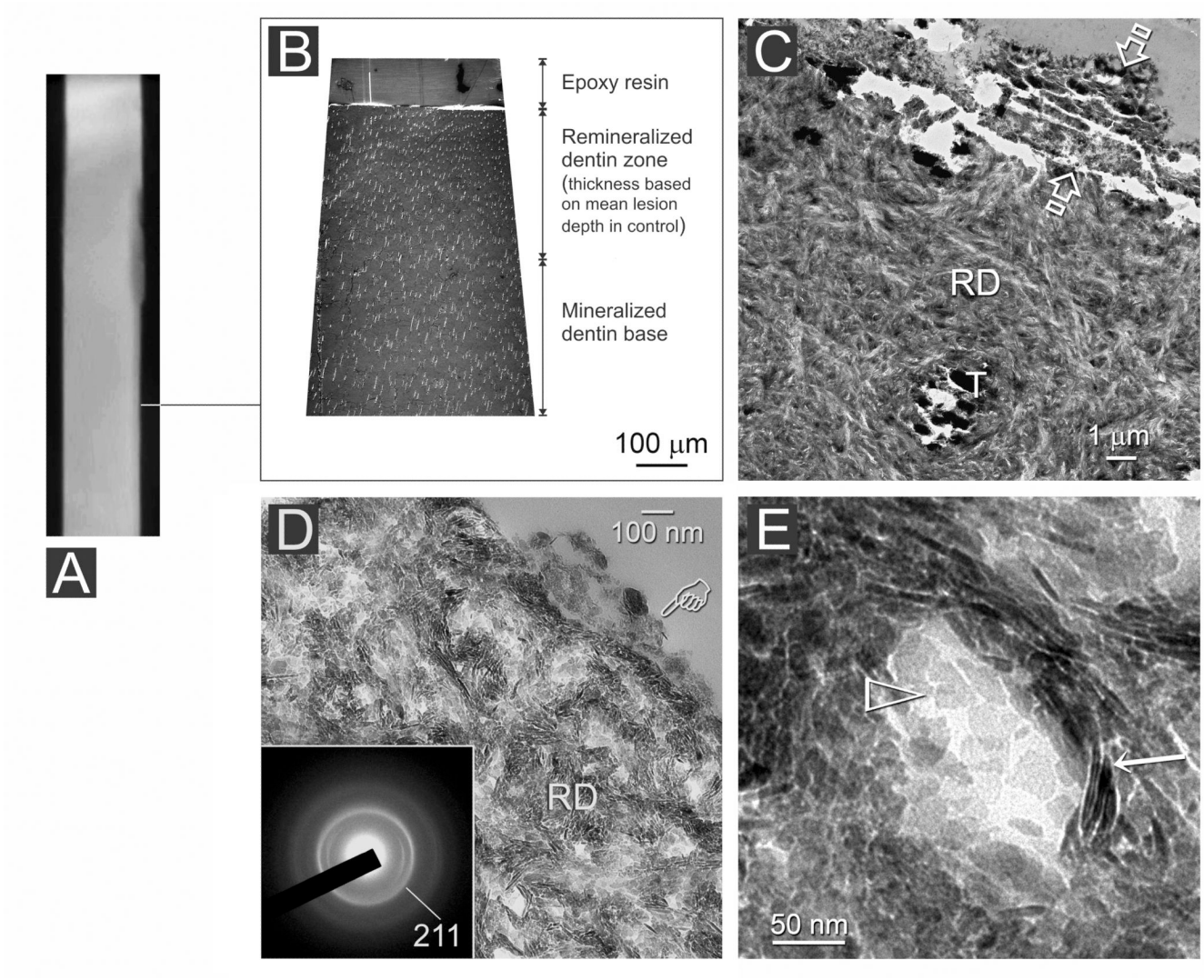

Fig. 4.

A non-bonded artificial caries-like dentin lesion after 4 months of biomimetic remineralization. **A**. A stacked 2-D micro-CT image indicating (line) the location from which TEM images were taken. **B**. Thick section of the remineralized lesion. At this magnification, there is no difference between the electron density of the remineralized dentin zone and the underlying mineralized dentin base. **C**. Thin section of the lesion surface with a layer of mineral precipitate (between open arrowheads). RD: Heavily remineralized dentin; T: dentinal tubule. **D**. Higher magnification of the remineralized dentin (RD) showing extrafibrillar and intrafibrillar remineralization. Pointer: surface mineral precipitates. Inset: selected area electron diffraction confirms the presence of apatite arranged along the longitudinal axis of the collagen fibrils. **E**. High magnification showing incomplete remineralization of the intrafibrillar space. Open arrowhead: intrafibrillar apatite platelets; Arrow: extrafibrillar apatite platelets.

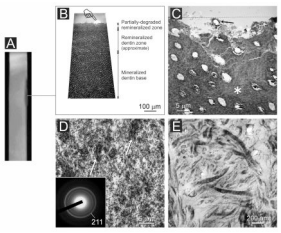

Fig. 5.

A. The same specimen as in Fig. 4 but with the TEM sections taken from a different location (line). **B**. Thick section showing slight decrease in electron density of the remineralized dentin zone when compared with the mineralized dentin base. Area indicated by the white halo (pointer) is shown at higher magnification in Fig. 5C. **C**. Non-demineralized thin section showing (dotted line) an area of degradation. A dentinal tubule (arrow) was suspended by partially-remineralized degraded dentin. Area indicated by the asterisk is shown at higher magnification in Fig. 5D. **D**. Area contains localized regions with denser remineralization (arrows) dispersed among regions with sparser mineralization. Inset: selected area electron diffraction indicates ring patterns indicative of a more random apatite arrangement. **E**. Stained demineralized thin section from the same tissue block. Areas with intact, cross-banded fibrils probably corresponded to the more heavily remineralized regions in Fig. 5D. Areas with degraded collagen probably corresponded to the sparsely remineralized regions.

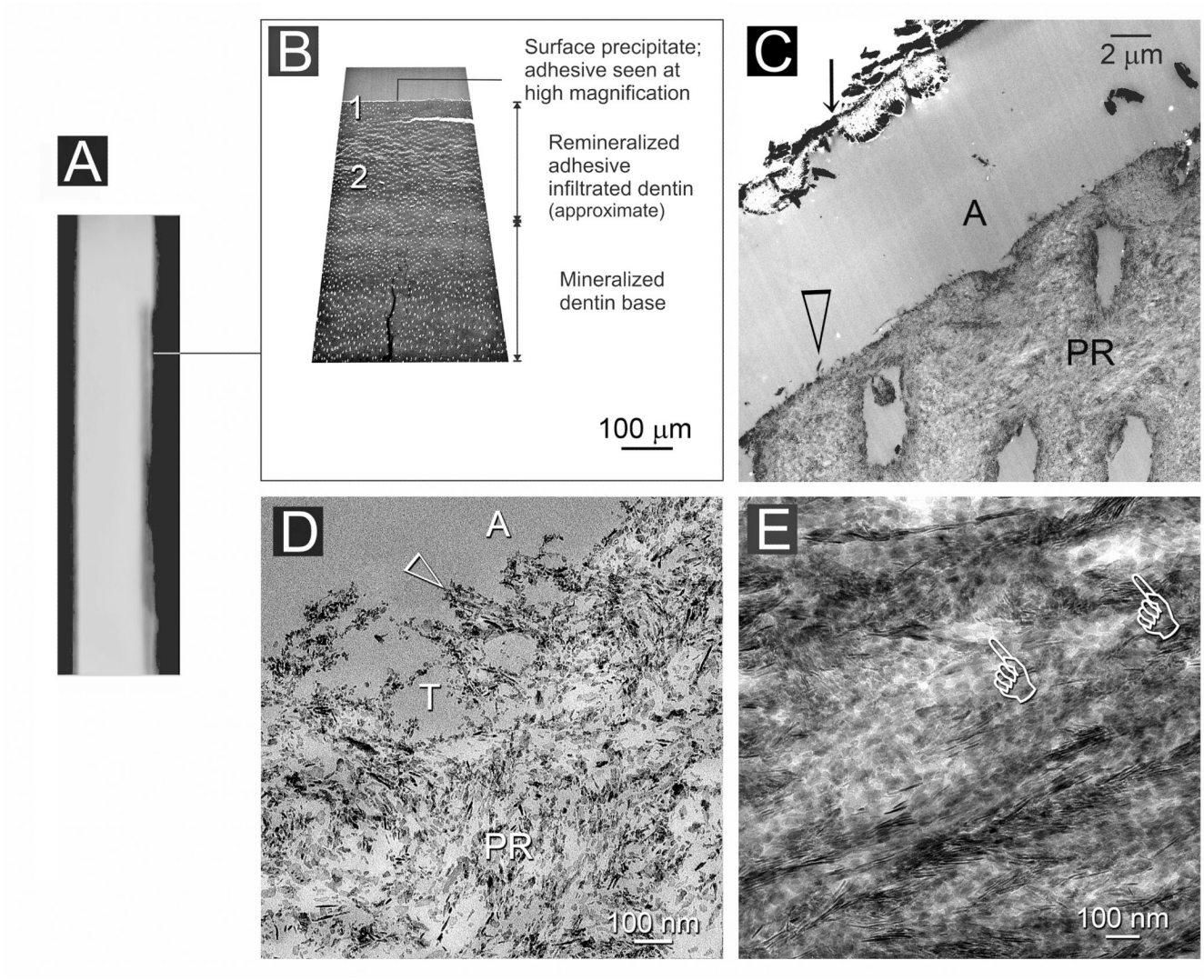

Fig. 6.

An adhesive infiltrated artificial caries-like dentin lesion after 4 months of biomimetic remineralization. **A**. A stacked 2-D micro-CT image indicating (line) the location from which TEM images were taken. **B**. Non-demineralized thick section showing a moderately remineralized zone of adhesive infiltrated dentin. The adhesive layer in this region could not be discerned at this magnification. **C**. Non-demineralized thin section showing a layer of mineral precipitate (arrow) over the adhesive (A). The surface of the lesion was partially-remineralized (PR). **D**. High magnification of the region indicated by "1" in Fig. 6B showing partial remineralization (PR) of the lesion surface, which, presumably, was better infiltrated by the dentin adhesive. Nevertheless, heavily remineralized shag carpet-like collagen fibrils could be seen along the dentin surface (open arrowhead). This feature is similar to the fibril depicted by the open arrowhead in Fig. 6B. A: adhesive; T: dentinal tubule. **E**. High magnification of the more hierarchical crystallite arrangement in the remineralized region depicted by "2" in Fig. 6B. Intrafibrillar compartments within incomplete apatite deposition are depicted by the pointers.

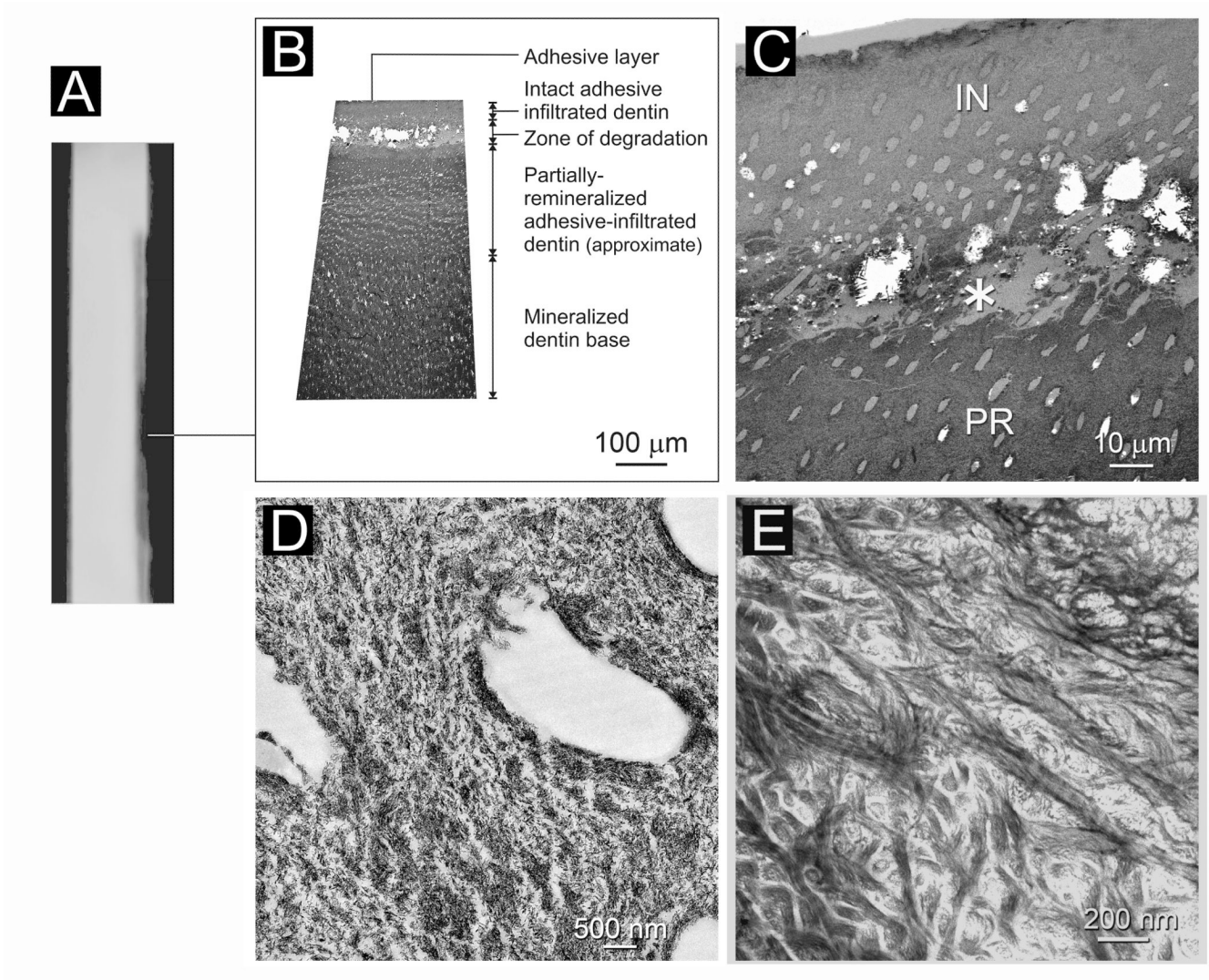

Fig. 7.

A. The same specimen as in Fig. 6 but with the TEM sections taken from a different location of the lesion (line). **B**. Non-demineralized thick section showing a region of intact adhesive infiltrated dentin along the lesion surface that is followed by a zone of collagen degradation. The part of the lesion beneath this zone of degradation was partially remineralized. **C**. Non-demineralized thin section of the lesion surface showing a 50 μm thick surface layer of intact adhesive infiltrated dentin (IN). Remineralization was sparse in this region except for the dentin surface. Beneath the surface intact region, there was a zone of collagen degradation (asterisk) where the dentin structure was incomplete. The part of the lesion beneath this region was partially-remineralized (PR). **D**. High magnification of the partially-remineralized degraded region indicated by the asterisk in Fig. 7C. **E**. Stained, demineralized thin section of the region corresponding to that indicated by the asterisk in Fig. 7C. Most of the collagen fibrils were degraded and were devoid of cross-banding patterns.

Dent Mater. Author manuscript; available in PMC 2012 May 1.

Table

Changes in lesion depth, lesion surface relative mineral content and ΔZ in artificial lesions (with or without dentin adhesive) remineralized biomimetically using sodium trimetaphosphate as a templating analog of matrix phosphoproteins

Parameter	Time period	Without adhesive * (N = 8)	With adhesive * (N = 8)
Lesion depth (μm)	Baseline	291.4 ± 7.3	291.9 ± 7.0
	1 month	211.8 ± 7.5	246.4 ± 26.4
	2 months	158.1 ± 19.3	205.8 ± 28.7
	3 months	119.7 ± 15.1	179.9 ± 24.6
	4 months	77.2 ± 9.4	138.6 ± 20.9
	Changes in lesion depth after 4 months (%)	**73.5 ± 3.0 [A]**	**52.6 ± 6.7 [B]**
Relative mineral content along lesion surface (vol%)	Baseline	11.1 ± 1.6	10.8 ± 1.1
	1 month	18.4 ± 1.8	12.0 ± 3.7
	2 months	26.4 ± 4.5	14.1 ± 2.8
	3 months	37.8 ± 4.3	18.0 ± 5.7
	4 months	41.4 ± 6.1	21.0 ± 8.7
	Changes in relative mineral content along lesion surface after 4 months (%)	**30.2 ± 2.9[a]**	**11.0 ± 3.5 [b]**
ΔZ (μm.vol%)	Baseline	5312.2 ± 409.6	5685.3 ± 248.8
	1 month	3704.2 ± 369.2	4998.8 ± 384.8
	2 months	2123.1 ± 430.0	4218.1 ± 537.2
	3 months	1127.8 ± 357.1	3390.0 ± 503.6
	4 months	489.4 ± 153.3	2486.0 ± 613.6
	Changes in ΔZ after 4 months (μm.vol%)	4822.9 ± 324.0	3198.4 ± 440.8
	**Remineralization efficacy after 4 months (%) ** **	**90.9 ± 2.5 [1]**	**56.6 ± 9.5 [2]**

* Values are means ± standard deviations. For each parameter summary, groups with different upper case letters, lower case letters or numerals are significantly different ($p < 0.05$)

** Remineralization efficacy = [$\Delta Z_{baseline} - \Delta Z_{4\ months}$)/$\Delta Z_{baseline}$*100%], where ΔZ represents the integrated mineral loss from the artificial carious lesion